J|A|C|S
ARTICLES
Published on Web 01/04/2007

Origin of the Monoclinic-to-Monoclinic Phase Transition and Evidence for the Centrosymmetric Crystal Structure of $BiMnO_3$

Alexei A. Belik,*,† Satoshi Iikubo,‡ Tadahiro Yokosawa,§ Katsuaki Kodama,‡ Naoki Igawa,‡ Shinichi Shamoto,‡ Masaki Azuma,||,⊥ Mikio Takano,|| Koji Kimoto,§ Yoshio Matsui,§ and Eiji Takayama-Muromachi†

Contribution from the Advanced Nano Materials Laboratory (ANML) and High Voltage Electron Microscopy Station (HVEMS), National Institute for Materials Science (NIMS), 1-1 Namiki, Tsukuba, Ibaraki 305-0044, Japan, Quantum Beam Science Directorate, Japan Atomic Energy Agency, Tokai, Ibaraki 319-1195, Japan, Institute for Chemical Research, Kyoto University, Uji, Kyoto-fu 611-0011, Japan, and PRESTO, Japan Science and Technology Corporation (JST), Kawaguchi, Saitama 332-0012, Japan

Received September 4, 2006; E-mail: Alexei.BELIK@nims.go.jp

Abstract: Structural properties of polycrystalline single-phased $BiMnO_3$ samples prepared at 6 GPa and 1383 K have been studied by selected area electron diffraction (SAED), convergent beam electron diffraction (CBED), and the Rietveld method using neutron diffraction data measured at 300 and 550 K. The SAED and CBED data showed that $BiMnO_3$ crystallizes in the centrosymmetric space group $C2/c$ at 300 K. The crystallographic data are $a = 9.5415(2)$ Å, $b = 5.61263(8)$ Å, $c = 9.8632(2)$ Å, $\beta = 110.6584(12)°$ at 300 K and $a = 9.5866(3)$ Å, $b = 5.59903(15)$ Å, $c = 9.7427(3)$ Å, $\beta = 108.601(2)°$ at 550 K, $Z = 8$, space group $C2/c$. The analysis of Mn−O bond lengths suggested that the orbital order present in $BiMnO_3$ at 300 K melts above $T_{OO} = 474$ K. The phase transition at 474 K is of the first order and accompanied by a jump of magnetization and small changes of the effective magnetic moment and Weiss temperature, $\mu_{eff} = 4.69\mu_B$ and $\theta = 138.0$ K at 300−450 K and $\mu_{eff} = 4.79\mu_B$ and $\theta = 132.6$ K at 480−600 K.

Multiferroic materials have received renewed interest in recent years.[1] In multiferroic systems, two or all three of (anti)-ferroelectricity, (anti)ferromagnetism, and ferroelasticity are observed in the same phase.[2] Such systems are rare in nature[2] but potentially studied with interest in wide technological applications.[1]

$BiFeO_3$[3] and $BiMnO_3$[4−19] have been extensively studied as multiferroic materials. $BiFeO_3$ is ferroelectric with the Curie temperature $T_E = 1123$ K and antiferromagnetic with the Néel temperature $T_N = 650$ K. $BiMnO_3$ is a unique compound among $BiBO_3$ (B = Cr,[4,20,21] Fe, Co,[22] and Ni[23]) because $BiMnO_3$ is the only one compound that shows true ferromagnetic ordering at $T_c = 99-105$ K.[4,8,10] In addition, orbital degrees of freedom are active in $BiMnO_3$.[6,8,19] However, it was difficult to show ferroelectricity in $BiMnO_3$ because of the lack of single crystals

† ANML, NIMS.
‡ Japan Atomic Energy Agency.
§ HVEMS, NIMS.
|| Institute for Chemical Research.
⊥ PRESTO.

(1) For recent reviews, see: (a) Eerenstein, W.; Mathur, N. D.; Scott, J. F. *Nature* **2006**, *442*, 759. (b) Khomskii, D. I. *J. Magn. Magn. Mater.* **2006**, *306*, 1. (c) Fiebig, M. *J. Phys. D: Appl. Phys.* **2005**, *38*, R123. (d) Hill, N. A. *Annu. Rev. Mater. Res.* **2002**, *32*, 1.
(2) Hill, N. A. *J. Phys. Chem. B* **2000**, *104*, 6694.
(3) Wang, J.; Neaton, J. B.; Zheng, H.; Nagarajan, V.; Ogale, S. B.; Liu, B.; Viehland, D.; Vaithyanathan, V.; Schlom, D. G.; Waghmare, U. V.; Spaldin, N. A.; Rabe, K. M.; Wuttig, M.; Ramesh, R. *Science* **2003**, *299*, 1719.
(4) Sugawara, F.; Iiida, S.; Syono, Y.; Akimoto, S. *J. Phys. Soc. Jpn.* **1968**, *25*, 1553.
(5) Tomashpol'skii, Y. Y.; Zubova, E. V.; Burdina, K. P.; Venevtsev, Y. N. *Inorg. Mater.* **1967**, *3*, 1861.
(6) Atou, T.; Chiba, H.; Ohoyama, K.; Yamaguchi, Y.; Syono, Y. *J. Solid State Chem.* **1999**, *145*, 639.
(7) Seshadri, R.; Hill, N. A. *Chem. Mater.* **2001**, *13*, 2892.
(8) Moreira dos Santos, A.; Cheetham, A. K.; Atou, T.; Syono, Y.; Yamaguchi, Y.; Ohoyama, K.; Chiba, H.; Rao, C. N. R. *Phys. Rev. B* **2002**, *66*, 064425.
(9) dos Santos, A. M.; Parashar, S.; Raju, A. R.; Zhao, Y. S.; Cheetham, A. K.; Rao, C. N. R. *Solid State Commun.* **2002**, *122*, 49.
(10) Kimura, T.; Kawamoto, S.; Yamada, I.; Azuma, M.; Takano, M.; Tokura, Y. *Phys. Rev. B* **2003**, *67*, 180401(R).
(11) Faqir, H.; Chiba, H.; Kikuchi, M.; Syono, Y.; Mansori, M.; Satre, P.; Sebaoun, A. *J. Solid State Chem.* **1999**, *142*, 113.
(12) Shishidou, T.; Mikamo, N.; Uratani, Y.; Ishii, F.; Oguchi, T. *J. Phys.: Condens. Matter* **2004**, *16*, S5677.
(13) Sharan, A.; Lettieri, J.; Jia, Y.; Tian, W.; Pan, X.; Schlom, D. G.; Gopalan, V. *Phys. Rev. B* **2004**, *69*, 214109.
(14) Chi, Z. H.; Xiao, C. J.; Feng, S. M.; Li, F. Y.; Jin, C. Q.; Wang, X. H.; Chen, R. Z.; Li, L. T. *J. Appl. Phys.* **2005**, *98*, 103519.
(15) Montanari, E.; Righi, L.; Calestani, G.; Migliori, A.; Gilioli, E.; Bolzoni, F. *Chem. Mater.* **2005**, *17*, 1765.
(16) Montanari, E.; Calestani, G.; Migliori, A.; Dapiaggi, M.; Bolzoni, F.; Cabassi, R.; Gilioli, E. *Chem. Mater.* **2005**, *17*, 6457.
(17) (a) Yang, H.; Chi, Z. H.; Li, F. Y.; Jin, C. Q.; Yu, R. C. *Phys. Rev. B* **2006**, *73*, 024114. (b) Chi, Z.; Yang, H.; Li, F.; Yu, R.; Jin, C.; Wang, X.; Deng, X.; Li, L. *J. Phys.: Condens. Matter* **2006**, *18*, 4371.
(18) Yang, C. H.; Koo, T. Y.; Lee, S. H.; Song, C.; Lee, K. B.; Jeong, Y. H. *Europhys. Lett.* **2006**, *74*, 348.
(19) Yang, C. H.; Koo, J.; Song, C.; Koo, T. Y.; Lee, K. B.; Jeong, Y. H. *Phys. Rev. B* **2006**, *73*, 224112.
(20) Niitaka, S.; Azuma, M.; Takano, M.; Nishibori, E.; Takata, M.; Sakata, M. *Solid State Ionics* **2004**, *172*, 557.
(21) Kim, D. H.; Lee, H. N.; Varela, M.; Christen, H. M. *Appl. Phys. Lett.* **2006**, *89*, 162904.
(22) Belik, A. A.; Iikubo, S.; Kodama, K.; Igawa, N.; Shamoto, S.; Niitaka, S.; Azuma, M.; Shimakawa, Y.; Takano, M.; Izumi, F.; Takayama-Muromachi, E. *Chem. Mater.* **2006**, *18*, 798.
(23) Ishiwata, S.; Azuma, M.; Takano, M.; Nishibori, E.; Takata, M.; Sakata, M.; Kato, K. *J. Mater. Chem.* **2002**, *12*, 3733.

and the low resistance of $BiMnO_3$ films, making it difficult to associate measured dielectric hysteresis loops to ferroelectricity instead of nonlinear dielectric losses.[13] The ferroelectric polarization of $BiMnO_3$ was measured to be 0.043 $\mu C/cm^2$ at 200 K.[9] The first principle calculations of the polarization using the reported structural parameters[8] gave 0.52 $\mu C/cm^2$.[12] The magnetocapacitance effect was observed below T_c leading to coupling between the ferroelectric and ferromagnetic orders.[10]

$BiMnO_3$ has a highly distorted perovskite-type structure at room temperature (rt).[6] It is believed to crystallize is space group $C2$ as determined by electron diffraction and subsequent structural analysis from neutron powder diffraction data.[6] $BiMnO_3$ undergoes two high-temperature phase transitions at 470 and 770 K.[4,10,14,16] The phase transition at 470 K is monoclinic-to-monoclinic without any detectable change in the symmetry.[10,16] It is accompanied by a thermal effect, abrupt changes of lattice parameters, a small jump of resistivity,[10] and an anomaly of dielectric constant.[14] The phase transition at 770 K is monoclinic-to-orthorhombic.[10,16] The origin of the high-temperature phase transitions in $BiMnO_3$ has not been determined yet. It was proposed that one of the phase transitions should be a ferroelectric-paraelectric phase transition.

$BiCrO_3$[20] and Bi_2NiMnO_6[24] were reported to be isostructural with $BiMnO_3$, and $BiScO_3$ was found to have the centrosymmetric $BiMnO_3$-related structure with space group $C2/c$.[25] It was recently shown that thin-films samples of $BiCrO_3$ exhibit antiferroelectric properties rather than ferroelectric ones.[21] This result suggests that $BiCrO_3$ has a centrosymmetric crystal structure.

In this work, we showed using selected area electron diffraction (SAED) and convergent beam electron diffraction (CBED) that our bulk $BiMnO_3$ sample crystallizes in space group $C2/c$. We determined the crystal structures of $BiMnO_3$ by the Rietveld method from neutron powder diffraction data measured at 300 and 550 K. The structural data suggested that the orbital order in $BiMnO_3$ melts above 474 K.

Experimental Section

Synthesis. A mixture of Bi_2O_3 (99.99%) and Mn_2O_3 with an amount-of-substance ratio of 1:1 was carefully ground in acetone and dried at 420 K for 3 days. The starting mixture was sealed in Au capsules. Then high-pressure cells, consisting of graphite heaters and dense $NaCl-ZrO_2$ parts surrounding the Au capsules and separating the Au capsules from graphite heaters, were assembled. Just before the high-pressure treatment, the high-pressure cells were dried at 370 K for 12 h under a vacuum. The synthesis was performed in a belt-type high pressure apparatus at 6 GPa and 1383 K for 60−70 min. After heat treatment, the samples were quenched to rt, and the pressure was slowly released. The resultant samples were black powder. X-ray powder diffraction (XRD) showed that the samples were single phased. Single-phased Mn_2O_3 was prepared by heating commercial MnO_2 (99.99%) in air at 923 K for 24 h. Bi_2O_3 was dried at 570 K before its use. The formation of the powder and single-phased $BiMnO_3$ samples (actually very small single crystals) can be explained by the fact that we used 6 GPa and the much higher synthesis temperature of 1383 K compared with 3−6 GPa and 723−1323 K reported in the literature.[6,8−10,14−17,26,27]

Thermal Analysis. Differential scanning calorimetry (DSC) curves of $BiMnO_3$ were recorded in closed aluminum capsules between 300 and 550 K at a heating−cooling rate of 10 K/min on an SII Exstar 6000 (DSC 6220) instrument.

Magnetic Properties. Magnetic susceptibilities, $\chi = \mathbf{M}/\mathbf{H}$, of $BiMnO_3$ were measured on a SQUID magnetometer (Quantum Design, MPMS) between 2 and 350 K in an applied field of 100 Oe and between 300 and 600 K in an applied field of 10 kOe using a furnace under both zero-field-cooled (ZFC) and field-cooled (FC) conditions. Isothermal magnetization measurements were performed between −50 and 50 kOe at 5 K.

SAED and CBED Studies. The bulk specimen was crushed and dispersed on a carbon thin film on a Cu grid for transmission electron microscopy. The SAED and CBED patterns were taken at 300 K using an analytical transmission electron microscope (Hitachi: HF-3000S) with a cold field emission gun operated at an accelerating voltage of 300 kV. The SAED and CBED patterns were taken from specimen areas of about 300 and 10 nm in diameters, respectively.

Neutron Powder Diffraction Experiments and Structure Refinements. Neutron powder diffraction data of $BiMnO_3$ were collected at 300 and 550 K with the high-resolution powder diffractometer (HRPD) installed at the JRR-3M reactor in JAEA, Tokai. The incident neutron wavelength was 1.8233(10) Å. About 5.4 g of the sample were loaded in a vanadium cell (diameter: 6.0 mm) in a furnace. The data were taken with a step of ca. 0.05° in a 2θ range between 2.5° and 162° with 64 ^{3}He detectors.

The neutron powder diffraction data were analyzed by the Rietveld method with RIETAN-2000.[28] The background was represented by a ninth-order Legendre polynomial. The pseudo-Voigt function of Toraya[29] was used as a profile function (we refined six profile parameters). Isotropic atomic displacement parameters, B, with the isotropic Debye−Waller factor represented as $\exp(-B \sin^2\theta/\lambda^2)$ were assigned to all the sites. Bound coherent scattering lengths, b_c, used for the structure refinements were 8.532 fm (Bi), −3.750 fm (Mn), and 5.803 fm (O).[30] The neuron diffraction pattern at 300 K contained very weak reflections from the vanadium cell. V was included as the second phase during the refinement. The neutron diffraction pattern at 550 K showed additional reflections from a furnace (Cu and very weak reflections from Al). Cu was taken into account during the refinement.

Results

Characterization of $BiMnO_3$. Figure 1 shows inverse magnetic susceptibilities and DSC curves of $BiMnO_3$ between 300 and 600 K. The phase transition at 474 K (from the peak position on the DSC curve on heating) is accompanied by a jump of magnetization. In the low-temperature (300−450 K) and high-temperature (480−600 K) regions, the $\chi^{-1}(T)$ data could be fit by the simple Curie−Weiss equation

$$\chi(T) = \frac{C}{T-\theta} \tag{1}$$

where C is the Curie constant and θ is the Weiss constant. The fitted parameters are $C = 2.751$ cm^3 K/mol and $\theta = 138.0$ K at 300−450 K and $C = 2.869$ cm^3 K/mol and $\theta = 132.6$ K at 480−600 K. The effective magnetic moment ($\mu_{eff} = (8C)^{1/2}$) was calculated to be 4.69μ_B per Mn^{3+} ion at low temperatures and 4.79μ_B at high temperatures. These values are close to the localized Mn^{3+} moment of 4.90μ_B. In the 300−450 K and 480−600 K regions, there was no difference between the ZFC and

(24) Azuma, M.; Takata, K.; Saito, T.; Ishiwata, S.; Shimakawa, Y.; Takano, M. *J. Am. Chem. Soc.* **2005**, *127*, 8889.
(25) Belik, A. A.; Iikubo, S.; Kodama, K.; Igawa, N.; Shamoto, S.; Maie, M.; Nagai, T.; Matsui, Y.; Stefanovich, S. Yu.; Lazoryak, B. I.; Takayama-Muromachi, E. *J. Am. Chem. Soc.* **2006**, *128*, 706.
(26) Chiba, H.; Atou, T.; Faqir, H.; Kikuchi, M.; Syono, Y.; Murakami, Y.; Shindo, D. *Solid State Ionics* **1998**, *108*, 193.
(27) Yang, H.; Chi, Z. H.; Yao, L. D.; Zhang, W.; Li, F. Y.; Jin, C. Q.; Yu, R. C. *J. Appl. Phys.* **2006**, *100*, 044105.
(28) Izumi, F.; Ikeda, T. *Mater. Sci. Forum* **2000**, *321−324*, 198.
(29) Toraya, H. *J. Appl. Crystallogr.* **1990**, *23*, 485.
(30) Sears, V. F. *International Tables for Crystallography*, 3rd ed.; Kluwer: Dordrecht, 2004; Vol. C, pp 445−452.

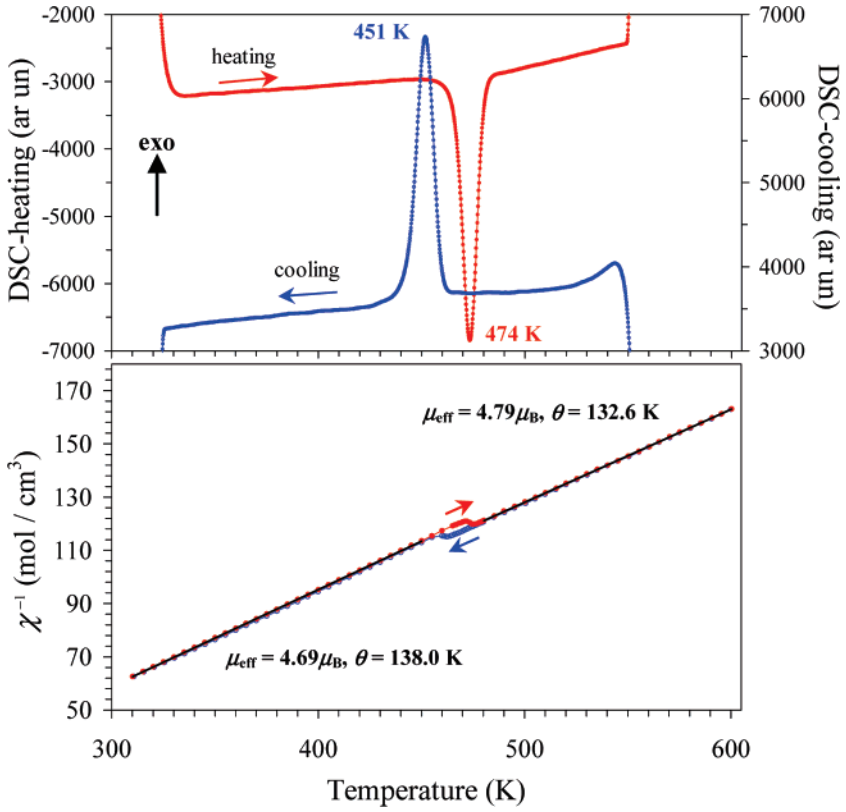

Figure 1. Dependence on temperature of (a) DSC curves for $BiMnO_3$ measured on heating (left-hand scale) and cooling (right-hand scale) and (b) the inverse magnetic susceptibility measured at 10 kOe for $BiMnO_3$ between 300 and 600 K. The solid lines in (b) show the fits by the Curie−Weiss equation. The parameters, μ_{eff} and θ, of the fits are given.

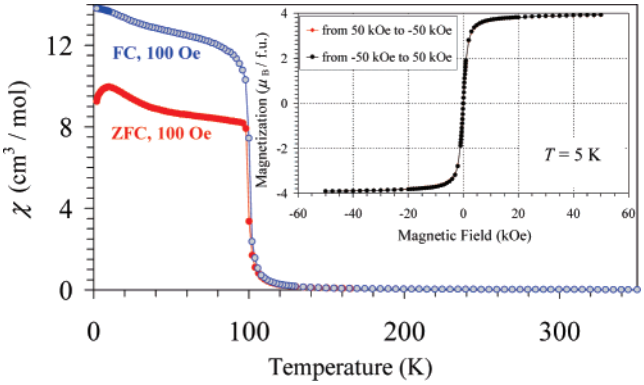

Figure 2. Temperature dependence of the magnetic susceptibilities measured at 100 Oe under ZFC and FC conditions between 2 and 350 K. Insert shows isothermal magnetization curves at 5 K between −50 and 50 kOe.

FC curves. A clear hysteresis was observed on the magnetic susceptibilities and DSC curves with the hysteresis of about 23 K for the DSC measurements. These data confirm that the phase transition is of the first order. The cycling of the DSC curves between 300 and 550 K gave reproducible results without any change in the peak positions and intensities.

Figure 2 shows the $\chi(T)$ curves below 350 K. The large difference was observed between the ZFC and FC curves below about 100 K with no difference above this temperature. A small temperature hysteresis was found near 100 K. At 5 K and 5 T (the inset of Figure 2), the magnetization reaches $3.92\mu_B$ per formula unit (f.u.) that is close to the fully aligned spin value of $4\mu_B$ for Mn^{3+}. The observed saturation value is larger than those reported in the literature.[10,14] A very small hysteresis is observed with the coercive field (H_c) of about 3 Oe and a remnant magnetization (M_r) of about $1.3 \times 10^{-2}\mu_B$ per Mn^{3+} ion. These values are much smaller than the previously reported ones, e.g., $H_c \approx 200-470$ Oe and $M_r \approx 0.2\mu_B$ for bulk samples[10,14,17] and $H_c \approx 400-1000$ Oe and $M_r \approx 0.5-1.0\mu_B$ for thin film samples.[18,31]

SAED and CBED of $BiMnO_3$. Figure 3 depicts a SAED pattern taken along the [010] zone axis. The reflections on the SAED patterns have been indexed based on the result of the previous neutron diffraction study in the monoclinic system.[6] The *hkl* ($h + k = 2n+1$) (these SAED patterns are not shown) and *h0l* ($l = 2n+1$) reflections are absent as indicated by arrows in Figure 3. The former extinction condition is due to that $BiMnO_3$ belongs to a *C*-centered monoclinic lattice.[32] The latter extinction condition is attributed to existence of a *c*-glide plane perpendicular to the *b*-axis.[32] Using CBED we also confirmed that the SAED pattern of Figure 3 was of the [010] incidence by observing the 2-fold rotational symmetry along the zone-axis, which enabled us to distinguish this pattern from the similar SAED patterns, e.g., [0−1−1]. The symmetry of CBED patterns including higher-order Laue zone (HOLZ) reflections yields information on three-dimensional symmetry elements of the crystal structure around the zone axis parallel to the incident beam direction. Figure 4 shows the [100] CBED pattern. The ring-shaped reflections around the center of the CBED pattern indicated by arrows stem from HOLZ. The HOLZ reflections clearly show the mirror-plane symmetry of the CBED pattern

(31) Eerenstein, W.; Morrison, F. D.; Scott, J. F.; Mathur, N. D. *Appl. Phys. Lett.* **2005**, *87*, 101906.
(32) *International Tables for Crystallography*, 5th ed.; Hahn, T., Ed.; Kluwer: Dordrecht, The Netherlands, 2002; Vol. A, p 52.

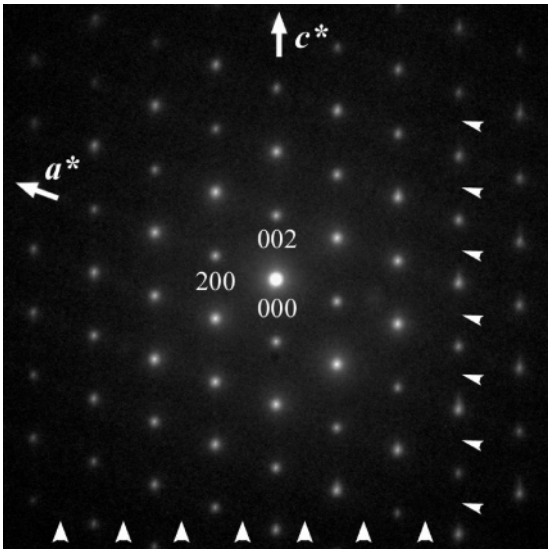

Figure 3. SAED pattern taken along the [010] zone axis. The $h0l$ ($h = 2n + 1$ and $l = 2n + 1$) reflections are absent due to the existence of the *C*-centered lattice and *c*-glide plane as indicated by arrows.

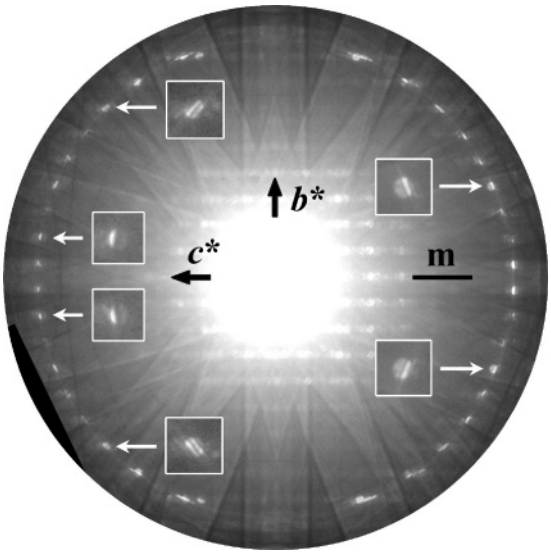

Figure 4. CBED pattern taken along the [100] zone axis. The HOLZ reflections clearly show the mirror-plane symmetry of this pattern perpendicular to the *b**-axis as indicated by the arrows.

perpendicular to the *b**-axis. Thus, it has been revealed that $BiMnO_3$ belongs to a point group 2/*m*. With the above SAED result, the space group of $BiMnO_3$ has been determined to be centrosymmetric *C*2/*c*.

It was reported that strong and long-time electron beam irradiation transforms the as-prepared monoclinic $BiMnO_3$ to new modifications characterized by different superstructures.[17,27] We used weak enough irradiation to prevent such a transformation. Note that when we increased the electron beam intensity and time, we indeed observed the transformations reported in the literature. It was also reported that there are different polymorphs in the as-prepared $BiMnO_3$ samples at room temperature found in the grain boundary regions by transmission electron microscopy.[15,26] However, in refs 17 and 27, it was suggested that different polymorphs are the results of strong electron beam irradiation because no polymorphism was found in those works. We also could not detect any polymorphism in the as-prepared $BiMnO_3$ samples under weak irradiation.

Table 1. Structure Parameters of $BiMnO_3$ at 300 and 550 K[a]

site	Wyckoff position	*x*	*y*	*z*	*B* (Å^2)
Bi	8*f*	0.136 38(13)	0.218 32(17)	0.126 17(13)	0.57(3)
		0.133 87(18)	0.2160(3)	0.1279(2)	1.47(4)
Mn1	4*e*	0	0.2115(6)	0.75	0.26(6)
		0	0.2326(8)	0.75	0.98(11)
Mn2	4*d*	0.25	0.25	0.5	0.67(7)
		0.25	0.25	0.5	0.96(11)
O1	8*f*	0.099 80(17)	0.1723(3)	0.581 45(16)	0.69(3)
		0.0892(3)	0.1865(5)	0.5886(3)	1.76(6)
O2	8*f*	0.145 78(18)	0.5714(3)	0.367 95(19)	0.90(3)
		0.1572(3)	0.5510(5)	0.3744(3)	2.56(7)
O3	8*f*	0.354 34(19)	0.5484(3)	0.164 71(18)	0.81(3)
		0.3529(3)	0.5487(4)	0.1586(3)	2.02(6)

[a] Space group *C*2/*c* (No 15); $Z = 8$; $a = 9.5415(2)$ Å, $b = 5.61263(8)$ Å, $c = 9.8632(2)$ Å, $\beta = 110.6584(12)°$, and $V = 494.24(2)$ Å^3, $R_{wp} = 3.61\%$ ($S = R_{wp}/R_e = 1.06$), $R_p = 2.82\%$, $R_B = 1.71\%$, and $R_F = 0.81\%$ at 300 K and $a = 9.5866(3)$ Å, $b = 5.59903(15)$ Å, $c = 9.7427(3)$ Å, $\beta = 108.601(2)°$, and $V = 495.63(3)$ Å^3, $R_{wp} = 4.20\%$ ($S = 1.10$), $R_p = 3.18\%$, $R_B = 2.64\%$, and $R_F = 1.52\%$ at 550 K. The occupation of all the sites is unity. The first (*x*, *y*, *z*, and *B*) line of each site is for 300 K, and the second is for 550 K.

Refinements of Crystal Structures of $BiMnO_3$. All the observed reflections on both neutron diffraction and XRD patterns of $BiMnO_3$ at 300 K could be indexed in the *C*2/*c* symmetry. The same reflection conditions were found at 550 K from the observed reflections on the neutron diffraction pattern. Structure parameters of $BiMnO_3$ at 300 and 550 K were successfully refined from neutron powder diffraction in space group *C*2/*c* using the fractional coordinates of $BiScO_3$[25] as the initial ones.

Final fractional coordinates, *B* parameters, lattice parameters, and *R* factors resulting from the Rietveld refinements are listed in Table 1. Selected bond lengths (l) and angles (ϕ) calculated with ORFFE,[33] bond valence sums (BVS),[34] and distortion parameters of MnO_6 octahedra (Δ)[35] are given in Table 2. Figure 5 displays observed, calculated, and difference neutron diffraction patterns.

Discussion

The SAED and CBED data confirmed that our bulk $BiMnO_3$ sample crystallizes in the centrosymmetric space group *C*2/*c* at 300 K. The observation of rather strong $h0l$ and $00l$ reflections with $l = 2n + 1$ on the $[1\bar{2}1]_p$,[15,26] $[01\bar{1}]_p$,[27] and $[\bar{1}10]_p$[17] zone axes (where p refers to the fundamental perovskite cell) in the previous works is likely due to the double diffraction. The possibility of the double diffraction was not mentioned and checked in those works. Space group *C*2 was assigned based on the observation of these reflections in the first papers by Chiba et al.[26] and Atou et al.[6] Note that we also observed strong $00l$ reflections with $l = 2n + 1$ on the [100] SAED pattern of $BiMnO_3$ (not shown here). However the [100] CBED zero-order Laue zone (ZOLZ) pattern clearly showed the dynamical extinction rule (GM-line) for the $00l$ reflections with $l = 2n + 1$ confirming the existence of the *c*-glide plane perpendicular to the *b**-axis. In addition, there are a number of very similar SAED patterns in $BiMnO_3$ making it difficult to assign a correct zone axis and, therefore, reflection indexes without the results

(33) Busing, W. R.; Martin, K. O.; Levy, H. A. *Report ORNL-TM-306*; Oak Ridge National Laboratory: Tennessee, 1964.
(34) Brese, R. E.; O'Keeffe, M. *Acta Crystallogr., Sect. B* **1991**, *47*, 192.
(35) Rodríguez-Carvajal, J.; Hennion, M.; Moussa, F.; Moudden, A. H.; Pinsard, L.; Revcolevschi A. *Phys. Rev. B* **1998**, *57*, 3189(R).

Table 2. Selected Bond Lengths, *l* (Å), Angles, ϕ (deg), Bond Valence Sums, BVS, and Distortion Parameters of MnO_6, Δ, in $BiMnO_3$[a]

	l, ϕ, BVS, and Δ	
	300 K	550 K
Bi−O2	2.218(2)	2.213(3)
Bi−O1	2.239(2)	2.304(3)
Bi−O3	2.246(2)	2.248(3)
Bi−O1a	2.466(2)	2.484(3)
Bi−O3a	2.710(2)	2.751(3)
Bi−O2a	2.837(2)	2.864(4)
Bi−O3b	3.003(2)	2.956(3)
Bi−O2b	3.077(2)	2.999(4)
Bi−O1b	3.148(2)	3.209(3)
Bi−O3c	3.265(2)	3.199(3)
BVS(Bi)	3.00	2.88
Mn1−O1 (×2)	2.199(2)	2.032(3)
Mn1−O2 (×2)	1.906(3)	2.011(4)
Mn1−O3 (×2)	1.986(3)	2.112(4)
BVS(Mn1)	3.05	2.75
Δ(Mn1−O)	37.2×10^{-4}	4.5×10^{-4}
Mn2−O1 (×2)	1.924(2)	2.024(3)
Mn2−O2 (×2)	2.242(2)	2.106(3)
Mn2−O3 (×2)	1.941(2)	1.913(3)
BVS(Mn2)	3.05	3.09
Δ(Mn2−O)	51.3×10^{-4}	15.4×10^{-4}
Mn1−O1−Mn2 (×2)	151.4(1)	150.9(1)
Mn1−O2−Mn2 (×2)	161.4(1)	158.3(1)
Mn1−O3−Mn2 (×2)	149.1(1)	152.0(1)

[a] BVS $= \sum_{i=1}^{N} v_i$, $v_i = \exp[(R_0 - l_i)/B]$, N is the coordination number, $B = 0.37$, $R_0(Bi^{3+}) = 2.094$, and $R_0(Mn^{3+}) = 1.76$;[34] $\Delta = (1/N) \sum_{i=1}^{N} [(l_i - l_{av})/l_{av}]^2$, where $l_{av} = (1/N) \sum_{i=1}^{N} l_i$ is the average Mn−O distance.[35]

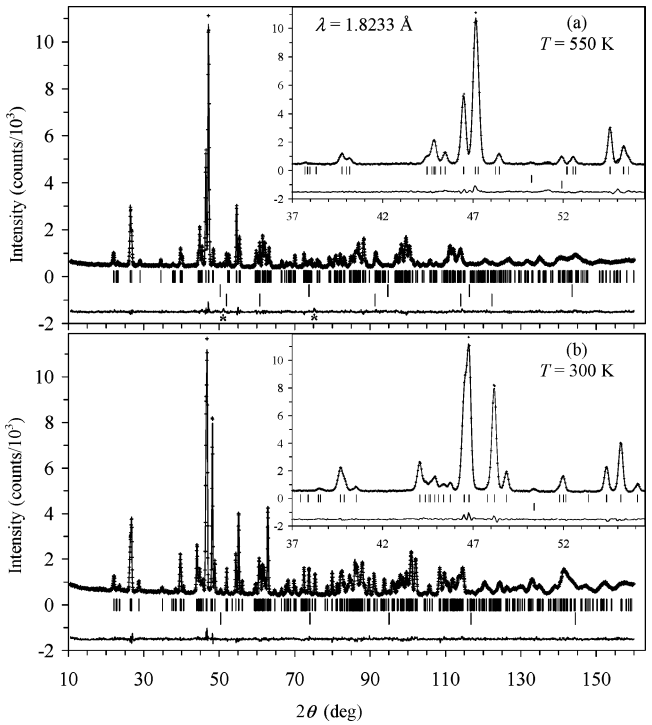

Figure 5. Observed (crosses), calculated (solid line), and difference patterns resulting from the Rietveld analysis of the neutron powder diffraction data for $BiMnO_3$ at (a) 550 K and (b) 300 K. Bragg reflections are indicated by tick marks. The lower tick marks are given for reflections from V. In (a), the third row of tick marks is given for reflections from a furnace, Cu; reflections from Al are shown by asterisks. Insets depict the enlarged fragments.

of CBED and determination of the incident direction. It is also possible that there is strong dependence of the structural properties of the bulk $BiMnO_3$ on the tiny changes of the stoichiometry and the appearance of Mn^{4+} or Mn^{2+} ions. Most of the previous works were done on samples containing different impurities. The tiny changes in the cation and oxygen stoichiometry can also explain the difference in the H_c, M_r, and saturated magnetization between our samples and the literature data for the bulk and thin films of $BiMnO_3$. For example, our studies on the $BiMn_{1-x}Sc_xO_3$ system showed that H_c and M_r are noticeably increased with increasing x up to $x = 0.2$ (and for $x = 0.05$: $H_c = 80$ Oe and $M_r = 0.27\mu_B$), while the saturated magnetization only slightly decreases.[36] In the case of thin-film samples, there exist additional compressive strains in films. In ref 16, it was suggested that the thin-film samples in reality consist of partially oxidized phases because these samples showed much lower ferromagnetic transition temperatures. The Bi-deficiency was found in thin-film samples by Rutherford backscattering spectroscopy,[37] and oxygen deficiency was suggested to explain the high conductivity of thin films.[38] All these facts can cause structural distortion from centrosymmetric to noncentrosymmetric.

There are other possible explanations of the contradiction between the centrosymmetric structure of $BiMnO_3$ and the observed second-harmonic generation[13,37] and magnetocapacitance effect.[10] The first one is that the centrosymmetric-to-noncentrosymmetric phase transition may occur at low temperatures in the magnetically ordered phase. An alternative suggestion is that the ferroelectric properties of $BiMnO_3$ originate from an electronic phase transition triggered by an electric field. The latter is supported by a giant increase (by 4 orders of magnitude) of the second-harmonic generation efficiency in thin-film $BiMnO_3$ samples under applied electric fields.[13] The possible relation between the orbital order and polarization was recently pointed out in $BiMnO_3$[19] and $LaMnO_3$ (having the average centrosymmetric structure with space group *Pnma*).[39] In $LaMnO_3$, the intrinsic dielectric anomalies were found at the orbital ordering temperature, and it was suggested that the polarization may develop locally because of orbital order.[39] Note that the first-principle calculations on $BiMnO_3$ showed that the centrosymmetric *C*2/*c* structure with zero polarization is more stable than the *C*2 structure at 0 K,[40] and $BiMnO_3$ was considered as antiferroelectric in the 1967s paper[5] and in ref 12.

To obtain information on formal oxidation states of Bi and Mn in $BiMnO_3$, we calculated their BVS (Table 2). The resulting BVS values were 3.00 for Bi and 3.05 for Mn1 and Mn2 at 300 K and 2.88 for Bi, 2.75 for Mn1, and 3.09 for Mn2 at 550 K, giving the oxidation state +3. At 300 K, almost ideal BVS values were obtained in the *C*2/*c* model compared with the BVS values calculated from the structure parameters reported in the literature for the *C*2 model (3.65 for Mn1 in ref 6 and 3.48 for the different site Mn3 in ref 8). Note that the analysis of our data in the *C*2 model gave more reasonable BVS values for the Mn sites (see Supporting Information).

(36) Belik, A. A.; Yokosawa, T.; Kimoto, K.; Matsui, Y.; Takayama-Muromachi, E., in preparation.
(37) Sharan, A.; An, I.; Chen, C.; Collins, R. W.; Lettieri, J.; Jia, Y. F.; Schlom, D. G.; Gopalan, V. *Appl. Phys. Lett.* **2003**, *83*, 5169.
(38) dos Santos, A. F. M.; Cheetham, A. K.; Tian, W.; Pan, X. Q.; Jia, Y. F.; Murphy, N. J.; Lettieri, J.; Schlom, D. G. *Appl. Phys. Lett.* **2004**, *84*, 91.
(39) Mondal, P.; Bhattacharya, D.; Choudhury, P. *J. Phys.: Condens. Matter* **2006**, *18*, 6869.
(40) (a) Baettig, P.; Spaldin, N. A. Private communication. (b) Shishidou, T.; Oguchi, T. Multiferroicity of $BiMnO_3$ reexamined from first principles. Presented at *APS March Meeting*, Baltimore, MD, 2006.

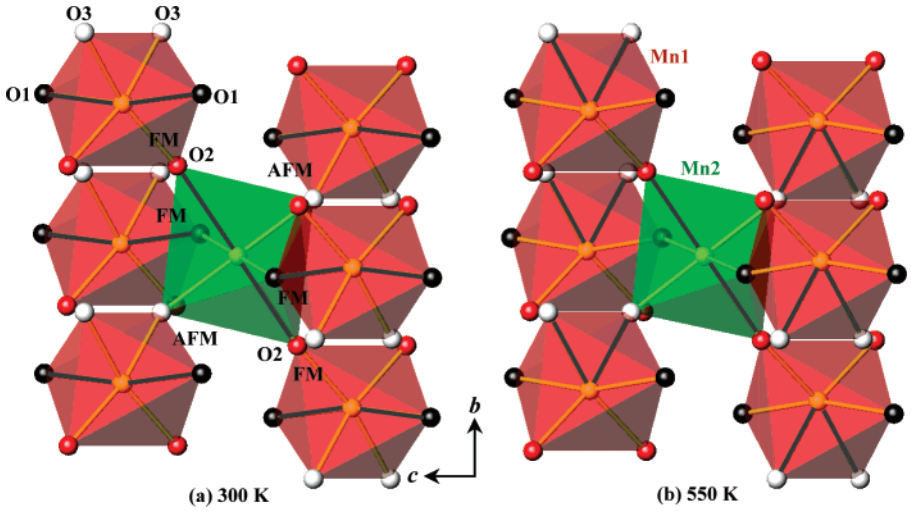

Figure 6. Fragments of the crystal structure of $BiMnO_3$ viewed along the *a*-axis at (a) 300 K and (b) 550 K; only MnO_6 octahedra are given. The black solid lines present the longest Mn−O bond lengths.

In the literature, the structure data of $BiMnO_3$ obtained in the *C*2 model had other problems, which were systematically ignored, in addition to the too large BVS values for some of the Mn sites. In the first paper reporting the crystal structure of $BiMnO_3$ from neutron powder diffraction at room temperature, estimated standard deviations (esd's) for atomic coordinates were too large for neutron powder diffraction data (for example, $(1-5) \times 10^{-3}$ for O).[6] This fact gives evidence for strong correlations between structural parameters in the *C*2 model.

Note that when we used the *C*2 model in the analysis of our data (see Supporting Information), esd's of atomic coordinates were also large (for example, $(0.8-4) \times 10^{-3}$ for O), and the O1 atom had a negative thermal parameter. The refinement of the structure at 550 K was very unstable (that is, small variations in nonstructural parameters and the *B* parameters had strong effects on the refined atomic coordinates) resulting in at least two minima with the same *R* factors but quite different bond lengths and BVS values (see Supporting Information). Therefore, the dispersion of Mn−O bond lengths was large in the *C*2 model, and it was very hard to detect the subtle differences between the structures at 300 and 550 K. The crystal structure of $BiMnO_3$ could also be refined in space group *Cc*. The *R* factors were the same in the *C*2 ($R_{wp} = 3.54\%$, $S = 1.04$, $R_p = 2.75\%$, $R_B = 1.63\%$, and $R_F = 0.76\%$ at rt) and *Cc* ($R_{wp} = 3.56\%$, $S = 1.05$, $R_p = 2.78\%$, $R_B = 1.65\%$, and $R_F = 0.77\%$ at rt) models and slightly smaller that those of the *C*2/*c* model ($R_{wp} = 3.61\%$, $S = 1.06$, $R_p = 2.82\%$, $R_B = 1.71\%$, and $R_F = 0.81\%$ at rt). It is explained by the fact that the number of refined structural parameters is two times larger in the *C*2 and *Cc* models. The same situation was found in the case of $BiScO_3$ (when the *R* factors were even smaller in the *Cc* model than those of the *C*2 model).[25] However, we have unambiguously shown using SAED, CBED, and second-harmonic generation studies that $BiScO_3$ crystallizes in space group *C*2/*c*.

At 300 K, the MnO_6 octahedra in $BiMnO_3$ are strongly distorted with two long distances (∼2.2 Å) and four short distances (∼1.95 Å). It is explained by the Jahn−Teller distortion of Mn^{3+} ions with d^4 configuration. The distortion parameters of MnO_6 octahedra (Table 2) are larger than that of $LaMnO_3$ at 300 K ($\Delta = 33.1 \times 10^{-4}$).[35] Such a strong distortion is associated with the orbital ordering. The ferromagnetism of $BiMnO_3$ is believed to stem directly from the particular orbital ordering.[6,8] Figure 6a shows the three-dimensional magnetic exchange between the Mn atoms at 300 K. The arrangements of orbitals revealed by the elongations of the MnO_6 octahedra in the *C*2/*c* model are the same as those proposed in refs 6 and 8 from the structural data obtained in the *C*2 model. According to the Goodenough−Kanamori rules, the superexchange interaction between Mn^{3+} ions becomes antiferromagnetic if both e_g orbitals point perpendicular to the bond direction, and the ferromagnetic interaction occurs if one of the e_g orbitals points along the bond direction; there should be four ferromagnetic interactions and two antiferromagnetic interactions (Figure 6a).[6,8] The ferromagnetic interactions were estimated to be larger than antiferromagnetic ones.[18] Because of the particular three-dimensional arrangements of strong ferromagnetic interactions (the antiferromagnetic Mn−O−Mn paths form one-dimensional zigzag chains along the [101] direction), the magnetic structure of $BiMnO_3$ is ferromagnetic below T_c.[8] This fact produces magnetic frustration. The ordered spin structure of $BiMnO_3$ is different from that of $LaMnO_3$, where four strong ferromagnetic interactions in plane and two antiferromagnetic interactions between planes result in the A-type antiferromagnetic structure.

At 550 K, the distortion of the MnO_6 octahedra in $BiMnO_3$ is considerably reduced as can be seen from the difference between the longest and shortest Mn−O distances (0.295 Å for Mn1 and 0.319 Å for Mn2 at 300 K and 0.104 Å for Mn1 and 0.194 Å for Mn2 at 550 K) and from the distortion parameters of MnO_6 octahedra (Δ, Table 2). However, there are still two long distances (∼2.1 Å) and four short distances (∼1.9−2.0 Å) at 550 K. The longest Mn1−O3 distances (2.113 Å) lie on one side of the Mn1 atom; that is, the O3−Mn1−O3 angle is 83.6° (Figure 6b). Therefore, the origin of the distortion of the $Mn1O_6$ octahedron is not the static Jahn−Teller effect. As a result, the long-range three-dimensional orbital ordering should be destroyed in $BiMnO_3$ at 550 K because of disappearance of the static Jahn−Teller distortion at least for one Mn site. Note that in $LaMnO_3$ after the melting of orbital ordering at $T_{OO} = 750$ K, the static Jahn−Teller distortion of the MnO_6 octahedron is completely removed ($\Delta \times 10^4$ changes from 33.1 to 0.9), and the structure transforms from orthorhombic to pseudo-cubic.[35] However, formally $LaMnO_3$ retains the same symmetry

above and below T_{OO} (space group *Pnma*). $BiMnO_3$ also retains the same symmetry (*C*2/*c*) below and above the phase transition temperature of 474 K. Despite the fact that the MnO_6 octahedra become much more regular in $LaMnO_3$ above T_{OO}, the tilt angle of the MnO_6 octahedra is conserved.[35] The same situation is observed in $BiMnO_3$ as can be seen from the Mn1−O−Mn2 bond angles at 300 and 550 K (Table 2).

The orbital melting in $LaMnO_3$ is accompanied by a jump in magnetic susceptibilities with the significant change in the Weiss constant and without any change in the Curie constant.[41] The Weiss constants are 177 and 52 K above and below T_{OO} in $LaMnO_3$. Considering two adjacent octahedra, there are nine possible orbital arrangements. However, three of them with parallel orbital configurations that give antiferromagnetic interactions are not favored from the viewpoint of optimal packing when orbital order is absent.[42] It should be noted that, in the six remaining orbital configurations, four ferromagnetic and two antiferromagnetic interactions are expected. That is the origin of the large positive Weiss constant of the $LaMnO_3$ above T_{OO}. The Weiss constant decreases below T_{OO} because the parallel orbital configurations along the *c* direction give relatively large antiferromagnetic interactions. In the case of $BiMnO_3$, there is also a jump in magnetic susceptibilities near $T_{OO} = 474$ K, but the change in the Weiss constant is quite small (Figure 1). The small jump of magnetic susceptibilities and small changes of the Weiss constant in $BiMnO_3$ compared with those of $LaMnO_3$ can be explained by the difference in the orbital ordering pattern. There is no parallel orbital configuration in the orbital ordering patterns of $BiMnO_3$, so the six orthogonal orbital arrangements with four ferromagnetic and two antifferomagnetic interactions do not change with or without the orbital order. Therefore smaller structural transformations in $BiMnO_3$ compared with those of $LaMnO_3$ are found from the changes in the Mn−O distances and the Δ parameters below and above the phase transition temperatures. Therefore, all anomalies observed at 474 K in $BiMnO_3$ resemble those of $LaMnO_3$ at 750 K, and the monoclinic-to-monoclinic phase transition in $BiMnO_3$ seems to have the same nature as the phase transition in $LaMnO_3$. The large difference between the orbital ordering temperatures of $BiMnO_3$ and $LaMnO_3$ may be explained by the presence of magnetic frustration in $BiMnO_3$ both above and below T_{OO} as discussed above and in ref 18 compared with unfrustrated interactions in the orbital ordered $LaMnO_3$.

It is interesting to note that the monoclinic β angles are similar in $BiMnO_3$ at 550 K (108.601°) and isostructural compounds $BiCrO_3$ (108.58°),[20] $BiScO_3$ (108.300°),[25] and Bi_2NiMnO_6 (107.823°)[24] at 300 K, where there is no orbital order. On the other hand, the β angle in $BiMnO_3$ at the orbital ordered state at 300 K (110.658°) differs noticeably from that at 550 K. Therefore, the value of the β angle may be an indicator of the presence of the orbital order in these systems. The structural phase transition from monoclinic-to-(pseudo)orthorhombic is observed in $BiMnO_3$ (at 770 K),[10] $BiCrO_3$ (at 420 K),[20] and Bi_2NiMnO_6 (at 485 K)[24] ($BiScO_3$ starts to decompose above 980 K[43] before this phase transition takes place). The monoclinic-to-monoclinic phase transition is found only in $BiMnO_3$ confirming that the orbital degrees of freedom play an important role in this transition.

Using the resonant X-ray scattering, the orbital melting temperature was determined to be 770 K that corresponds to the monoclinic-to-orthorhombic phase transition.[19] We have investigated the $BiMn_{1-x}Sc_xO_3$ system and found that the monoclinic-to-monoclinic phase transition disappears at $x = 0.05$.[36] The temperature of the magnetic phase transition decreases and the temperature of the monoclinic-to-orthorhombic phase transition increases with increasing *x*. The decrease of the magnetic phase transition temperature is in agreement with the dilution effect. However, it is highly unlikely that the orbital melting temperature, if it will be associated with the monoclinic-to-orthorhombic phase transition, will rise with increasing Sc content in $BiMn_{1-x}Sc_xO_3$. Therefore, these data also support the idea that the orbital melting takes place above 474 K and corresponds to the monoclinic-to-monoclinic phase transition.

In conclusion, the SAED and CBED data confirmed that $BiMnO_3$ has the *C*2/*c* symmetry at 300 K. This result is very important for theoretical studies of $BiMnO_3$ and structurally related compounds and in practical applications. Neutron diffraction allowed us to detect subtle differences between the structures of $BiMnO_3$ at 300 and 550 K. The application of the centrosymmetric *C*2/*c* model was essential to detect the subtle structural differences. We found, from our structural analysis and magnetization measurements, that orbital order disappears upon heating at $T_{OO} = 474$ K in $BiMnO_3$.

Acknowledgment. We thank Prof. D. I. Khomskii for valuable discussions and comments.

Supporting Information Available: Details of the structure refinements of $BiMnO_3$ in the *C*2 and *Cc* models (Tables S1−S6 and Figure S1). This material is available free of charge via the Internet at http://pubs.acs.org.

JA0664032

(41) Zhou, J. S.; Goodenough, J. B. *Phys. Rev. B* **1999**, *60*, 15002(R).
(42) Khomskii, D. I.; Kugel, K. I. *Phys. Rev. B* **2003**, *67*, 134401.
(43) Belik, A. A.; Azuma, M.; Takayama-Muromachi, E., unpublished results.